PNAS
www.pnas.org

Supplementary Information for

Experience-dependent plasticity in an innate social behavior is mediated by hypothalamic LTP

Stefanos Stagkourakis[1]*, *Giada Spigolon*[2], *Grace Liu*[1], *David J. Anderson*[1,3]*

***Corresponding author information:** Stefanos Stagkourakis, David J. Anderson
Email: stefanos.stagkourakis@caltech.edu, wuwei@caltech.edu

This PDF file includes:

Supplementary Information text
Figures S1 to S5 with legends
Table S1
SI References

www.pnas.org/cgi/doi/10.1073/pnas.2011782117

Supplementary Information Text

Extended Discussion

The plasticity observed at AHiPM→VMHvl^{Esr1} synapses likely has both post- and pre-synaptic components, as suggested by an increase in the AMPAR/NMDAR ratio (1-3) following aggression training (Fig. 2J, K), and by the differential responses of VMHvl^{Esr1} neurons to trains of pre-synaptic stimuli (4, 5) (Fig. 2L, M), respectively. Surprisingly, the form of hypothalamic LTP studied here does not exhibit "occlusion," phenomenon observed in studies of hippocampal or amygdalar LTP (6, 7), in which following *in vivo* behavioral induction of LTP in the synaptic population of interest, the magnitude of LTP that can be induced subsequently *ex vivo* is markedly decreased (Fig. 4D, K). Similarly, we do not observe the related phenomenon in which prior *in vivo* LTP can enhance the extent of LTD that can be induced *ex vivo* in slices from such animals. The reason(s) for the failure to observe these phenomena are not clear, and will require further studies to elucidate. There are a number of effects, however, which could account for these observations. Firstly, it is possible that the proportion of synapses modified by the *in vivo* social experience was small compared to the synapses being sampled in the slice. Another possibility is that the synapses being assayed in the slice are a different population than the ones modified *in vivo*, or lastly that new synapses were formed by the *in vivo* experience and they are the ones primarily contributing to the LTP and LTD being measured *in vitro*. This last possibility is of particular interest, given that - as presented in Fig. 3, an increase in spine density occurs in VMHvl^{Esr1} neurons of AGG mice.

The data on LTP presented here, blur the distinction between neural circuits mediating learned vs. innate behaviors, and reinforce the concept of "learned innate behavior," in which plasticity within developmentally hardwired circuits can function to modify the strength of an instinctive behavior in response to social experience (8, 9). An example of the latter in an invertebrate is the post-mating response in *Drosophila,* a form of memory in which female sexual receptivity is inhibited following mating (10-12).

This idea notwithstanding, more complex forms of learning, such as classical or operant conditioning, may utilize circuits that are parallel to those that mediate innate forms of the modified behavior, as shown in the case of conditioned *vs*. innate fear (13-15). In this context, it is worth noting that mice can learn an instrumental, operant response using successful aggressive encounters as a reinforcer (16), and that performance of this instrumental task is facilitated by optogenetic activation of VMHvl neurons (17). The neural substrates and synaptic mechanisms underlying this operant conditioning remain to be elucidated, although the nucleus accumbens-based reward system has been implicated in recent studies (18).

Aggressiveness can be enhanced not only by repeated successful agonistic encounters, as shown here, but also by prior mating experience (19). Recently, we showed that as little as 30 minutes of free social interaction with a female was sufficient to transform a socially naive mouse into an AGG mouse within 24 hrs of the interaction (8). This effect was associated with a change in the neural representation of male *vs*. female conspecifics among VMHvl^{Esr1} neurons, from partially overlapping to largely non-overlapping (8). Whether this change in neural population coding involves synaptic plasticity within VMHvl, or is inherited from upstream structures, such as the MeA (9), remains to be determined. In other studies, we have shown that the effect of social isolation stress to promote aggression in non-sexually experienced males is mediated by the neuropeptide Neurokinin B (NkB) and its receptor Nk3R, acting in the dorso-medial hypothalamus (DMH) (20). The relationship of this form of experience-dependent plasticity to VMHvl^{Esr1} neuronal activity is currently unknown.

Our current findings also provide insights into individual differences in the ability of genetically identical animals to respond to “aggression training”. Firstly, we show here that several physiological parameters in AGG mice are different from those in socially naïve mice. These include elevated baseline VMHvl^{Esr1} neuron activity (Fig. 1G-J), increased spontaneous excitatory input onto VMHvl^{Esr1} neurons (Fig. 2A-C), increased AMPA/NMDA ratio at AHiPM→VMHvl^{Esr1} synapses (Fig. 2I-K) and altered synaptic integration properties (Fig. L, M). By contrast, in NON mice the spontaneous inhibitory inputs to VMHvl^{Esr1}

neurons are increased, relative to socially naïve mice (Fig. S1). In addition, NON mice exhibit shorter lasting LTP and longer lasting LTD than are observed in AGG mice (Fig. 4D, G). Whether increased LTD is sufficient to account for the failure of NON mice to respond to aggression training is not yet clear. Another possibility, suggested by the increased spontaneous IPSCs, is that VMHvl receives stronger inhibitory input from GABAergic neurons in NON mice. While there are very few GABAergic neurons within VMHvl itself (21), VMHvl receives strong inhibitory input from the neighboring tuberal (TU) region. It is possible that the lack of aggression in NON mice reflects potentiation of these TU GABAergic neurons. The synaptic mechanisms responsible for the lack of aggression in NON mice will clearly require further investigation.

We also find that NON mice have lower levels of circulating T in comparison to AGG mice, and that experimental administration of supplemental T can restore the capacity for "aggression learning" in such animals. While the role of T in promoting male aggressiveness is well-established (22-27), our studies provide new insight into the neurophysiological mechanisms that may mediate this effect in the context of aggression training. Specifically, we observe that NON animals can only express LTP *in vivo* following administration of exogenous T. Although LTP can be induced optogenetically *ex vivo* in slices from control NON animals, LTP in slices from T-implanted NON animals exhibited higher-amplitude and persistence. Moreover, in AGG mice, levels of T increased during aggression training. This correlation suggests either that T acts directly to enhance LTP at this synapse, which in turn promotes aggression, or that T acts indirectly, by promoting aggressive behavior which in turn enhances LTP (Fig. S5). Whether T directly influences synaptic plasticity, and if so the underlying molecular mechanisms involved, as well as the mechanistic basis of individual differences in T levels, are interesting topics for future study.

Our experiments have focused on a specific glutamatergic input to $VMHvl^{Esr1}$ neurons which have a causal role in aggression. In addition to our findings, recent work reported that VMHvl-projecting $Vglut^{+}$ neurons in the AHiPM are active during both social investigation and attack, and that functional manipulation of these neurons influences attack (28, 29). $VMHvl^{Esr1}$ neurons receive inputs from neurons

in over 30 different structures (30), raising the question of whether other glutamatergic inputs to these cells also display plasticity. Indeed, recently published work has identified synaptic plasticity promoted by foot-shock stress in a medial amygdala projection that primarily targets the central part of VMH (VMHc) (31). Although a causal role in promoting aggression was not directly demonstrated for this input, and the mechanism of potentiation was not established, plasticity at this synapse may regulate stress-induced aggression (31). The present study demonstrates that AHiPM→ VMHvl^{Esr1} synapses can undergo Hebbian LTP, and that potentiation of these synapses occurs during social experience that enhances offensive aggression. Together, these data suggest that VMHvl likely provides a substrate in which aggression plasticity can occur at multiple synaptic inputs, each of which may play distinct roles in physiology and/or behavior. Our results also reveal striking effects of aggression training on dendritic spine morphology among VMHvl^{Esr1} neurons, although we cannot be certain whether the secondary dendritic branches where we observe this phenomenon receive synaptic input from AHiPM. Other recent studies have identified structural plasticity among VMHvl^{PR}-derived axons innervating hypothalamic targets in females, which are mediated by changes in sex steroids during estrus (32). The present work, together with these other studies, begins to provide a view of the acute and dynamic changes that can occur through experience and/or hormonal modulation, in a brain node that controls innate social behaviors.

Extended Materials and Methods

Animals. All mice were housed in ventilated micro-isolator cages in a temperature-controlled environment (median temperature 23 °C), under a reversed 12h dark-light cycle, and had *ad libitum* access to food and water. Mouse cages were changed weekly on a fixed day on which experiments were not performed.

Brain slice electrophysiology. Acute mouse brain slices were prepared. Slices were cut on a vibratome (Leica VT1000S) to 300 µm thickness and continuously perfused with oxygenated aCSF containing (in millimolar): NaCl (127), KCl (2.0), NaH_2PO_4 (1.2), $NaHCO_3$ (26), $MgCl_2$ (1.3), $CaCl_2$ (2.4), and D-glucose (10). See also *SI Appendix,* Table S1. Whole-cell current- and voltage-clamp recordings were performed with micropipettes filled with intracellular solution containing (in millimolar), K-gluconate (140), KCl (10), HEPES (10), EGTA (10), and Na_2ATP (2) or Cesium methanesulfonate (140), KCl (10), HEPES (10), EGTA (10), and Na_2ATP (2) (pH 7.3 with KOH). Recordings were performed using a Multiclamp 700B amplifier, a DigiData 1440 digitizer, and pClamp 11 software (Molecular Devices). Slow and fast capacitative components were semi-automatically compensated. Access resistance was monitored throughout the experiments, and neurons in which the series resistance exceeded 15 MΩ or changed ≥20% were excluded from the statistics. The liquid junction potential was 9.7 mV and not compensated. The recorded current was sampled at 20 kHz. Baseline recordings of EPSCs, IPSCs and optogenetically-evoked synaptic currents were performed in normal aCSF conditions and in the absence of GABA and NMDA receptor blockers. Spontaneous excitatory currents were sampled at the reversal of Cl^- (V_{HOLD}=-70 mV), and spontaneous inhibitory currents were sampled at the reversal of fast excitatory neurotransmission (V_{HOLD}=0 mV). All recordings were performed at near-physiological temperature (33±1ºC). Reagents used in slice electrophysiology experiments; Neurobiotin™ tracer (Vector laboratories) was used in combination with Streptavidin conjugated to Alexa Fluor 647. MATLAB and OriginPro9 were used for electrophysiological data analysis. CNQX (10 µM), D-AP5 (25 µM), TTX (500 nM), and 4-AP (100 mM) were bath applied to block excitatory transmission and to test if optogenetically evoked responses are monosynaptic (28). All drugs were pre-applied for 5 min in the slice chamber prior to data acquisition.

Brain slice Ca^{2+} imaging. The spontaneous activity of mouse $VMHvl^{Esr1}$ neurons was monitored by imaging fluorescence changes of the jGCaMP7s biosensor, using a CCD camera (Evolve® 512, Photometrics), mounted on an Olympus BX51WI microscope. Recordings were 5 min in duration. As a

subpopulation of VMHvl^{Esr1} neurons likely expresses T-type Ca^{2+} channels, the Ca^{2+} transients reported in Fig. 1 reflect both action potentials and subthreshold synaptic potentials. A 60x water-dipping objective was used to focus on VMHvl. Ca^{2+} imaging analysis was performed using the MIN1PIPE one-photon based calcium imaging signal extraction pipeline (30), in combination with custom-written MATLAB routines.

Cell filling and reconstruction. Mouse *Esr1*$^{+}$ VMHvl neurons were recorded in whole-cell mode with intracellular pipette solution as above, with the addition of 0.2% neurobiotin. After recording, slices were placed in fixative (4% paraformaldehyde/0.16% picric acid), washed in PBS and incubated at 4°C for 72h in a solution containing streptavidin conjugated to Alexa Fluor 647. After extensive washing, slices were mounted with 2.5% DABCO in glycerol. VMHvl^{Esr1} neuron identity of all filled cells was confirmed with colocalization studies of viral-induced tdTomato expression.

***Ex vivo* optogenetics.** Photostimulation during slice whole-cell recordings was performed via a 3.4 watt 535 nm LED mounted on the microscope fluorescence light source and delivered through the 60X objective's lens. Photostimulation was controlled via the analog outputs of a DigiData 1440A, enabling control over the duration and intensity. The photostimulation diameter through the objective lens was ~310 μm with illumination intensity typically scaled to 0.35 mW/mm^2.

***In vivo* optogenetics.** Subjects were coupled via a ferrule patch cord to a ferrule on the head of the mouse using a zirconia split sleeve (Doric Lenses). Ferrules and fiber-optic patch cords were purchased from Thorlabs and Doric Lenses, respectively. The optical fiber was connected to THORLABS fiber-coupled LED (M530F2, 9.6 mW) via a fiber-optic rotary joint (FRJ_1x1_FC-FC, Doric Lenses) to avoid twisting of the cable caused by the animal's movement. Prior to a testing session, following the coupling of the patch cords with the optic fiber ferrules, *Esr1*$^{Cre/+}$ animals were given 10 min to acclimate in their home cage in the absence of an intruder. The frequency and duration of photostimulation were controlled using the programmable train generator Pulse Pal (31). Light power was controlled by dialing an analog

knob on the LED driver (T-Cube™ LED Driver with Trigger Mode, Thorlabs, LEDD1B). Light power was measured from the tip of the ferrule in the patch cord at different laser output settings, using an optical power energy meter and a photodiode power sensor (Thorlabs, PM100D, and S130VC). Light power was dialed at 0.5 mW at the fiber tip. Upon identification of the fiber placement coordinates in brain tissue slides, irradiance (light intensity) was calculated using the brain tissue light transmission calculator based on (http://www.stanford.edu/group/dlab/cgi-bin/graph/chart.php) using laser power measured at the tip and the distance from the tip to the target brain region measured by histology. Animals showing no detectable viral expression in the target region and/or ectopic fiber placement were excluded from the analysis.

***In vivo* electrophysiology.** *In vivo* electrophysiology recordings were performed in freely moving mice, using chronic silicon probe implants. All extracellular recordings were conducted in the left VMHvl, and all mice included in the present study were validated using the following criteria: identification of the lipophilic dye (DiD) tract targeting VMHvl, phototagging of VMHvl^{Esr1} neurons, and photostimulation-evoked low-latency attack against a conspecific through optrode mediated VMHvl^{Esr1} neuron photoactivation. Recordings were performed using an optrode based on the A1x32-Poly2-10mm-50s-177 NeuroNexus probe and a 100 µm optic fiber placed along the probe's shank terminating 50 µm above the probe's first recording sites. Photostimulation was delivered using fiber-coupled Thorlabs LEDs (M530F2, 9.6 mW for LTP/LTD studies, and M617F2, 13.2 mW for phototagging), and light power was dialed at 0.33 mW at the optrode's fiber tip. The probe was implanted 200 µm above the intended recording site, and using the NeuroNexus OH32LP oDrive was lowered over a period of four days to the target coordinates (lowering by 50 µm/day). Only channels that showed photo-responses in the local field potential were used for LFP analysis. Recordings were performed using the Open Ephys acquisition board with a sampling rate of 30 kHz, the Open Ephys I/O board, and the Open Ephys GUI (31). The LFP signal was obtained by applying low pass-filtering with a cut-off at 100 Hz on the raw voltage traces. Note that although the excitation wavelength for testing LTP *in vivo* was chosen to preferentially activate

AHiPM synaptic input to VMHvl neurons via Chronos, due to spectral overlap between the opsins we cannot exclude a contribution of direct ChrimsonR-mediated Esr1 neuron activation to the fEPSPs.

Immunohistochemistry. Mice were anesthetized with ketamine (KetaVed, VEDCO) and xylazine (AnaSed, NDC 59399-110-20), then transcardially perfused with 20 mL of ice-cold fixative. Whole brains were dissected, immersed in ice-cold fixative for 90 min then stored in 0.1M PBS (pH 7.4) containing 20% sucrose, 0.02% bacitracin and 0.01% sodium azide for three days, before freezing with dry ice. Coronal sections were cut at a thickness of 14 µm on a cryostat (Microm, Walldorf) and thaw-mounted onto gelatine-coated glass slides. For GFP staining, brain sections were incubated overnight at 4°C using a chicken anti-GFP antibody (Aves Labs, Inc., GFP-1010) at 1:500 dilution. For tdTomato staining brain sections were incubated overnight at 4°C using a rabbit anti-DsRed antibody (Takara, 632392) at 1:500 dilution. Primary antibody incubation was followed by Alexa-488-conjugated goat anti-chicken secondary antisera (1:500; Invitrogen), and/or Alexa-568-conjugated donkey anti-rabbit secondary antisera (1:500; Invitrogen). DAPI solution (1mg/mL) was used at 1:10000 dilution. For further details on reagents, see also *SI Appendix*, Table S1.

Confocal microscopy. Brain slices were imaged by confocal microscopy (Zeiss, LSM 800). Brain areas were determined according to their anatomy using Paxinos and Franklin Brain Atlas (8, 33).

For cell reconstructions, each entire neurobiotin-filled neuron was acquired at 63X (NA = 1.4), 1 µm step size using a Zeiss LSM880 confocal microscope. Imaris 9.3 (Bitplane) was used to visualize the topology of the dendritic tree and the centrifugal branch ordering method was chosen to sort dendrites, assigning order 1 to the root. 2nd order dendrites were then selected for further imaging acquisition to perform spine quantification. 70-90 µm-long dendritic segments were acquired at 63X (NA = 1.43), 0.1 µm step size and 0.06x0.06 pixel-size using Airy-scan detector at the LSM880. Two segments were acquired for dendrites longer that 200 µm.

For spine quantification, images of dendritic segments were rendered in Imaris using the *Blend* algorithm and the *Filament* module was used to reconstruct dendrites and spines. Specifically, the auto-path method was chosen and thinnest spine diameter (between 1.5 and 2 μm), maximal distance from the dendrite (between 3 and 8 μm) and fluorescence intensity threshold were defined in every single dendrite to detect spines. The statistics module in Imaris was used to extract spine density values. Three to six segments per neuron were quantified and values were averaged.

Tail-tip whole blood sampling. Whole blood samples of 40-70 μL were collected from the lateral tail vein of restrained mice (32). Only blood samples acquired within 2 min post-restraining were used for hormone measurements, and the subjects were then returned to their home cage. Briefly, the rodent's tail was immersed for 30 sec in 40^{o}C water to dilate the tail blood vessels. Immediately after, a 23G needle was used to puncture the lateral tail vein, and whole blood was collected. Bleeding was stopped via applying gentle pressure to the tail at the level of the puncture with surgical cleaning tissue, and 2% chlorhexidine antiseptic solution was used for tail disinfection at the end of the procedure. Blood samples were refrigerated at 4^{o}C for 30 min and then centrifuged at 4^{o}C at 2000 RCF. Following centrifugation, serum was collected and was frozen at -80^{o}C for a maximal period of 2 months prior to performing ELISA measurements. All blood samples were acquired during the dark phase of the 12h/12h light/dark cycle. For further details on reagents, see also *SI Appendix*, Table S1.

Testosterone ELISA. 96-well plates were used in a ready-to-use kit for testosterone ELISA (R&D systems – Catalog number KGE010). Linear regression was used to fit the optical densities for the standard curve *vs* the concentration. The standard curve range for corticosterone was 300 to 100000 pg/mL. Concentrations were calculated from the optical density at 450 nm of each sample. Appropriate sample dilutions were carried out to maintain detection in the linear part of the standard curve and typically involved 1 to 10 for mouse serum samples. Data acquired from the performed ELISAs are presented as absolute values. Differences between groups were identified by Student's *t*-test or ANOVA.

Viral vectors. For *ex vivo* Ca^{2+} imaging studies of VMHvl neurons, *Esr1Cre/+* male mice were injected in VMHvl with 200 nL of AAV9-Syn-FLEX-jGCaMP7s-WPRE (addgene 104491-AAV9) 5.3×10^{12} genomic copies per mL. For *ex vivo* optogenetic studies, *Esr1Cre/+* male mice were injected in VMHvl with 200 nL of AAV9-FLEX-tdTomato (addgene 28306-AAV9) 4.2×10^{12} genomic copies per mL and in AHiPM with 100 nL of AAV5-Syn-Chronos-GFP (addgene 59170-AAV5) 3.7×10^{12} genomic copies per mL. For *in vivo* optogenetic and electrophysiology experiments, *Esr1Cre/+* male mice were injected in VMHvl with 100 nL of AAV5-Syn-FLEX-rc[ChrimsonR-tdTomato] (addgene 62723-AAV5) 4.1×10^{12} genomic copies per mL and in AHiPM with 100 nL of AAV5-Syn-Chronos-GFP (addgene 59170-AAV5) 3.7×10^{12} genomic copies per mL. Control groups were injected in VMHvl with 100 nL of AAV9-FLEX-tdTomato (addgene 28306-AAV9) 4.2×10^{12} genomic copies per mL and in AHiPM with 100 nL of AAV5-CAG-GFP (37825-AAV5) 5.9×10^{12} genomic copies per mL. For further details on reagents, see also *SI Appendix*, Table S1.

Stereotactic surgery and viral gene transfer. Adult heterozygous *Esr1Cre/+* males were single-housed for at least five days before undergoing surgical procedures and were operated on at 16–20 weeks of age. Mice were anesthetized using isoflurane (5% induction, 1–2% maintenance, in 95% oxygen) and placed in a stereotaxic frame (David Kopf Instruments). Body temperature was maintained using a heating pad. An incision was made to expose the skull for stereotaxic alignment using the inferior cerebral vein and the Bregma as vertical references. We based the coordinates for the craniotomy and stereotaxic injection of VMHvl on an anatomical magnetic resonance atlas of the mouse brain (AP: −4.68 mm; ML: ±0.78 mm; DV: −5.80 mm), as previously described (34). Virus suspension was injected using a pulled-glass capillary at a slow rate of 8–10 nL/min, 100 nl per injection site (Nanojector II, Drummond Scientific; Micro4 controller, World Precision Instruments). The glass capillary was withdrawn 10 min after the cessation of injection.

Osmotic mini-pumps. Testosterone was dissolved at 30 mg/ml in sesame oil and was administered for 2 weeks at a rate of 0.75 mg/hour via subcutaneous osmotic mini-pumps (Alzet, model 1002) (35). For further details on reagents, see also *SI Appendix*, Table S1.

Social behavior assays. The aggression phenotype of animals defined as aggressive (AGG), or non-aggressive (NON) in the present study was based on the expression of aggressive behavior in the five consecutive day resident-intruder test (5cdRI). Animals that did not express any aggressive behavior in the 5cdRI were identified as NONs, while all AGGs expressed aggression in a minimum of three out of the five trials, with the majority expressing attack behavior in all five days. As described in Fig. 1, the 5cdRI composed of a 15 min social interaction test per day in the resident's home arena, with socially naïve 4-5 month-old residents. Intruders were BALB/c males 2-3 months old and of lower weight/size. Three follow up tests were performed in the 5cdRI experimental design presented in Fig. 1, specifically, 2 weeks, 4 weeks and 12 weeks following the completion date of the 5cdRI assay. Note that only 15 out of a total of 106 aggressive mice, were used to quantify the effect of aggression training. This was based on the finding that following behavioral analysis of the first 15 mice used in the study, the power of the ANOVA test reached $P < 0.0001$. This suggested that including additional observations would not aid the power of the statistical test. In Fig. 5, following the 5cdRI, on day six a social interaction test was performed in a novel home-cage-sized arena. In addition to the C57 male, a male with a larger bodyweight/size CD-1 conspecific was introduced. The duration of this experiment was 15 min, following which both animals were returned to their home cage.

Statistics. No statistical methods were used to predetermine sample sizes but our sample sizes are similar to those reported in previous publications (36). Data met the assumptions of the statistical tests used and were tested for normality and variance. Normality was determined by D'Agostino–Pearson normality test. All *t*-tests and one-way ANOVAs were performed using GraphPad Prism software (Graphpad Software Inc.). Statistical significance was set at $P < 0.05$.

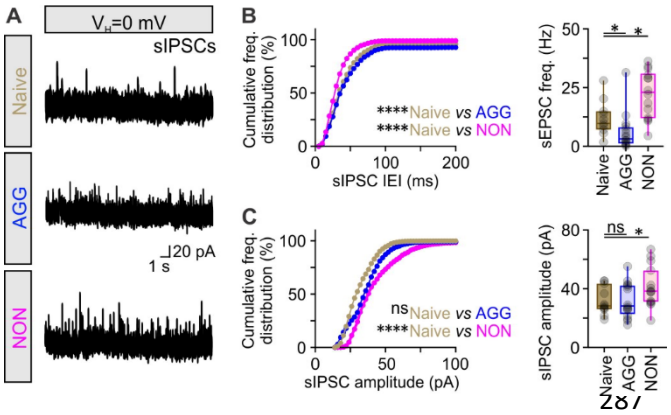

Fig. S1. Presynaptic plasticity of inhibitory input in VMHvl^{Esr1} neurons of non-aggressive male mice.

(A) Representative recordings of spontaneous inhibitory post-synaptic currents (sIPSCs) from VMHvl^{Esr1} neurons, from socially naive, aggressive (AGG) and non-aggressive (NON) mice.

(B) Left – cumulative frequency distribution plot of sIPSC inter-event interval (IEI) in voltage-clamp recordings collected from VMHvl^{Esr1} neurons from socially naive, AGG and NON mice (n=11-14 VMHvl^{Esr1} neuron recording per group, collected from 8-10 mice per group, Kolmogorov-Smirnov test, $P < 0.0001$ between socially naive and AGG mice, $P < 0.0001$ between socially naive and NON mice). Right – comparison of sIPSC frequency in voltage-clamp recordings collected from VMHvl^{Esr1} neurons from socially naive, AGG and NON mice (n=11-14 VMHvl^{Esr1} neuron recording per group, collected from 8-10 mice per group, Kruskal-Wallis one-way ANOVA with uncorrected Dunn's post hoc test, $P = 0.0425$ between socially naive and AGG mice, $P = 0.0480$ between socially naive and NON mice).

(C) Left – cumulative frequency distribution plot of sIPSC amplitude in voltage-clamp recordings collected from VMHvl^{Esr1} neurons from socially naive, AGG and NON mice (n=11-14 VMHvl^{Esr1} neuron recording per group, collected from 8-10 mice per group, Kolmogorov-Smirnov test, $P = 0.2780$ between socially naive and AGG mice, $P < 0.0001$ between socially naive and NON mice). Right – comparison of sIPSC amplitude in voltage-clamp recordings collected from VMHvl^{Esr1} neurons from socially naive, AGG

and NON mice (n=11-14 VMHvl^{Esr1} neuron recording per group, collected from 8-10 mice per group, Kruskal-Wallis one-way ANOVA with uncorrected Dunn's post hoc test, $P = 0.8995$ between socially naive and AGG mice, $P = 0.0476$ between socially naive and NON mice).

ns; not significant, *$P < 0.05$, ****$P < 0.0001$. In box plots the median is represented by the center line, the interquartile range is represented by the box edges, the bottom whisker extends to minimal value, and the top whisker extends to the maximal value.

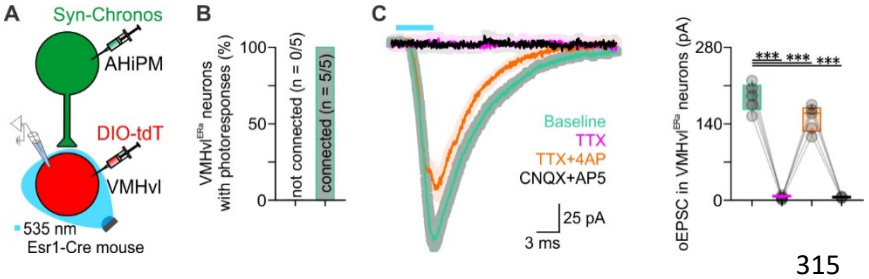

315

316 **Fig. S2. Monosynaptic connectivity between AHiPM and VMHvl^{Esr1} neurons.**

317 (A) Schematic illustration of the experimental design, transducing AHiPM neurons with Chronos and
318 optically evoking postsynaptic responses in VMHvl^{Esr1} neurons *ex vivo*.

319 (B) Quantification of VMHvl^{Esr1} neurons with optically-evoked EPSCs (oEPSCs).

320 (C) Averaged amplitudes of oEPSCs evoked on baseline (green), TTX (magenta), TTX + 4AP (orange),
321 and in CNQX and AP5 (black); n=5 brain slices, collected from n=5 mice, one-way ANOVA with Dunnett's
322 post hoc test, P = 0.0002 between baseline and TTX conditions, P = 0.0001 between baseline and
323 TTX+4AP conditions, P = 0.0002 between baseline and CNQX+AP5 conditions. Shaded region
324 represents the standard error. The vertical scale bar defines current and the horizontal scale bar time.

325 ***P < 0.001. In box plots the median is represented by the center line, the interquartile range is
326 represented by the box edges, the bottom whisker extends to minimal value, and the top whisker extends
327 to the maximal value.

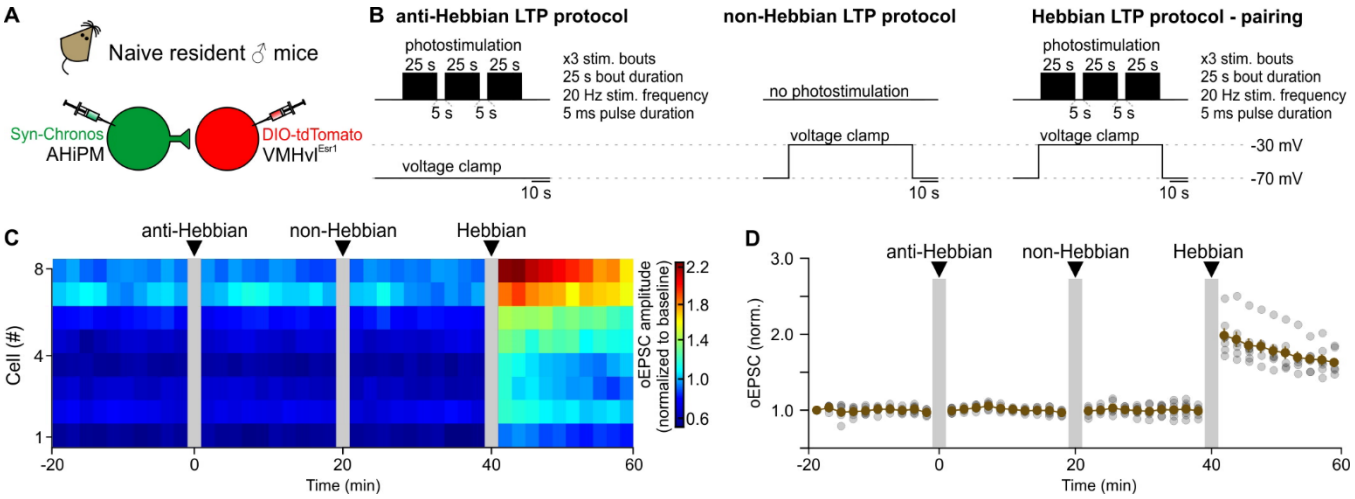

Fig. S3. Characterization of LTP-inducing stimulation protocols at the AHiPM→VMHvl^{Esr1} synapse.

(A) Schematic of the experimental design used to identify the appropriate stimulation protocol for LTP induction *ex vivo* in socially naïve mice.

(B) Illustration of the experimental protocols tested to to induce LTP in the AHiPM→VMHvl synapse.

(C) Monitoring the optically induced EPSC (oEPSC) prior to, and following application of each of three stimulation protocols (n=8 cells, n=5 socially naïve mice).

(D) Alternative quantification/illustration of optically induced EPSC (oEPSC) prior to, and following application of each of three stimulation protocols (n=8 cells, n=5 socially naïve mice – similar to panel C).

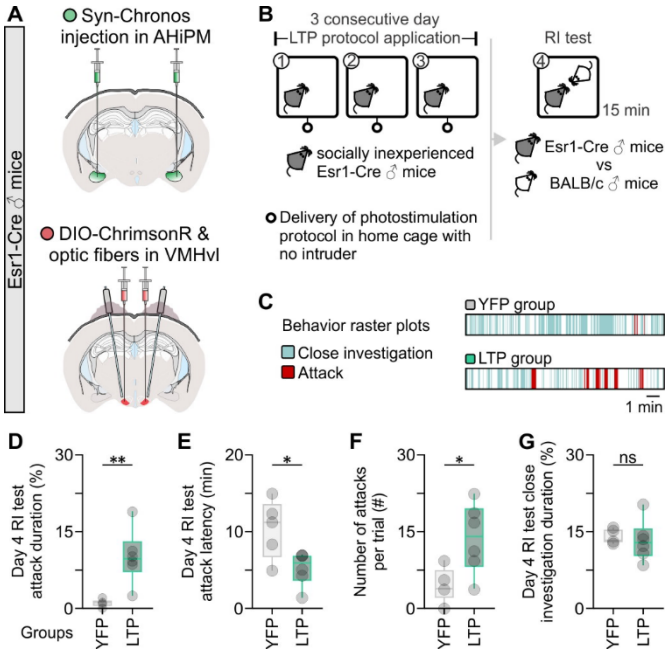

345

346 **Fig. S4. Optogenetic induction of LTP at AHiPM→VMHvl^{Esr1} synapses in socially naïve mice leads**

347 **to elevated aggression in the first resident-intruder test.**

348 (A) Schematic indicative of the experimental design used to induced hypothalamic LTP in the

349 AHiPM→VMHvl synapses, via Chronos-eYFP expression in AHiPM, and ChrimsonR expression in

350 VMHvl^{Esr1} neurons.

351 (B) Schematic of the behavior test design used to identify whether induction of LTP in the AHiPM→VMHvl

352 synapses, influences the innate expression of aggression.

353 (C) Representative behavior raster plots of a control (YFP) and opsin-expressing (LTP) mouse, in the

354 resident-intruder test against a novel BALBc conspecific.

355 (D) Quantification of attack duration (n=5-6 mice per group, two-tailed unpaired *t*-test, $P = 0.0046$ between

356 YFP and LTP groups).

(E) Quantification of attack latency (n=5-6 mice per group, two-tailed unpaired *t*-test, $P = 0.0214$ between YFP and LTP groups).

(F) Quantification of number of attacks per trial (n=5-6 mice per group, two-tailed unpaired *t*-test, $P = 0.0235$ between YFP and LTP groups).

(G) Quantification of close investigation duration (n=5-6 mice per group, two-tailed unpaired *t*-test, $P = 0.7106$ between YFP and LTP groups).

$^{*}P < 0.05$, $^{**}P < 0.01$. In box plots the median is represented by the center line, the interquartile range is represented by the box edges, the bottom whisker extends to minimal value, and the top whisker extends to the maximal value.

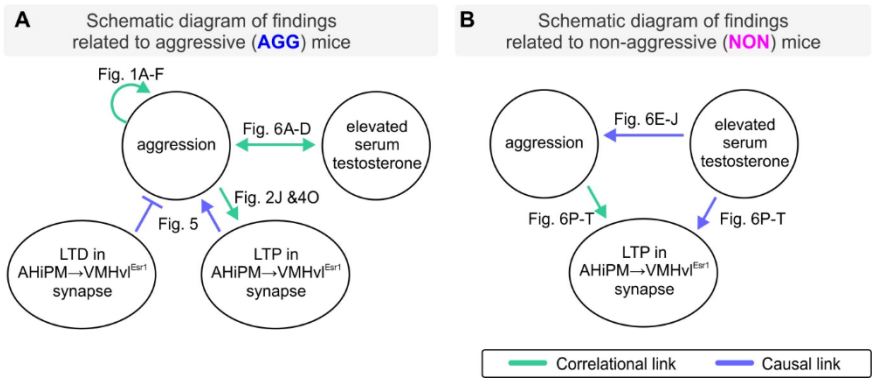

371

372 **Fig. S5. Schematic summary.**

373 (A) The schematic summarizes the findings from AGG mice, and the suggested links between
374 aggression, serum testosterone and hypothalamic LTP.

375 (B) Similar to panel (A), but summarizing results from experiments in NON mice - this schematic
376 summarizes the identified links among aggression, serum testosterone and hypothalamic LTP. Our
377 results do not distinguish whether the effect of elevated serum testosterone to increase LTP *in vivo* (Fig.
378 6P-T) is direct, or rather indirect via an effect to increase aggressive behavior, which in turn enhances
379 LTP. However, exogenous administration of T to NON mice (in the absence of any aggressive
380 experience) enhances LTP amplitude and persistence as tested *ex vivo* (Fig. 6K-O).

Materials and Methods

Table S1. Reagents and resources.

REAGENT or RESOURCE	SOURCE	IDENTIFIER
Antibodies		
Rabbit monoclonal anti-DsRed	Takara	632392
Anti-GFP rabbit serum	Invitrogen	A-6455
Chicken polyclonal anti-GFP	Aves Labs, Inc.	GFP-1010
Donkey anti-Mouse IgG- Alexa Fluor 488	ThermoFisher	A-21202
Donkey anti-Rabbit IgG- Alexa Fluor 488	ThermoFisher	A-21206
Donkey anti-Rabbit IgG- Alexa Fluor 568	ThermoFisher	A-10042
Donkey anti-Rabbit IgG- Alexa Fluor 647	ThermoFisher	A-31573
Goat anti-Chicken IgY- Alexa Fluor 488	ThermoFisher	A-11039
Biotinylated Goat Anti-Rabbit IgG Antibody	Vector Laboratories	BA-1000
Donkey anti-Rabbit IgG- Alexa Fluor 568	ThermoFisher	A-10042
Chemicals, Peptides, and Recombinant Proteins		
Picric acid	Sigma-Aldrich	P6744
4% paraformaldehyde (PFA) in PBS	Santa Cruz Biotech.	CAS30525-89-4
Streptavidin conjugated to Alexa Fluor 647	ThermoFisher	CS32357
Neurobiotin tracer	VectorLabs	SP-1120-50
Sodium chloride	Sigma-Aldrich	S9888
Sodium bicarbonate	Sigma-Aldrich	S6297
D-(+)-Glucose	Sigma-Aldrich	G7528
Sodium phosphate monobasic dihydrate	Sigma-Aldrich	71505
Potassium chloride	Sigma-Aldrich	P9333
Magnesium sulfate heptahydrate	Sigma-Aldrich	63138
Calcium chloride dihydrate	Sigma-Aldrich	C5080
4-Aminopyridine	Sigma-Aldrich	275875
CNQX disodium salt	TOCRIS	1045
D-AP5	TOCRIS	0106

Tetrodotoxin citrate	Alomone labs	T-550
DAPI solution (1mg/mL)	ThermoFisher	62248
OCT Cryomount	Histolab	45830
Normal donkey serum (NDS)	Sigma-Aldrich	D9663
Bovine Serum Albumin (BSA)	Sigma-Aldrich	A2153
Triton X-100	Sigma-Aldrich	T8787
Sucrose	Sigma-Aldrich	S7903
DiD' solid	Invitrogen	D7757
Vectastain ABC kit	Vector Laboratories	PK-6100
3,3-Diaminobenzidine tetrahydrochloride hydrate (DAB)	Sigma-Aldrich	D5637
Testosterone	Sigma-Aldrich	T1500
Sesame oil	Sigma-Aldrich	S3547-250ML
Phosphate buffer saline (PBS)	Santa Cruz Biotech.	SC-24946
ELISA kit		
Testosterone Parameter Assay Kit	R&D systems	KGE010
Experimental Models: Organisms/Strains		
Esr1$^{Cre/+}$	Lee et al., 2014	Own breeding
BALB/cAnNCr mouse line	Charles River	https://www.criver.com/
Crl:CD1(ICR)	Charles River	https://www.criver.com/
AAV mediated gene transfer		
AAV5-CAG-GFP	addgene	37825-AAV5
AAV9-FLEX-tdTomato	addgene	28306-AAV9
AAV5-Syn-Chronos-GFP	addgene	59170-AAV5
AAV5-Syn-FLEX-rc[ChrimsonR-tdTomato]	addgene	62723-AAV5
AAV9-Syn-FLEX-jGCaMP7s-WPRE	addgene	104491-AAV9
Software		
Clampfit 11	MOLECULAR DEVICES	https://www.moleculardevices.com/
MATLAB 2018	MathWorks	https://www.mathworks.com/

OriginPro 9	OriginLab	https://www.originlab.com/
ImageJ	NIH; Schneider et al., 2012	https://imagej.nih.gov/ij/
Prism 8	GraphPad	https://www.graphpad.com/scientific-software/prism/
Illustrator CC 2020	Adobe Systems	http://www.adobe.com
CorelDrawX8	CorelDRAW graphics suite	https://www.coreldraw.com/
Photoshop 2020	Adobe Systems	http://www.adobe.com

383

References for extended discussion and extended materials and methods

1. J. A. Kauer, R. C. Malenka, Synaptic plasticity and addiction. *Nature reviews. Neuroscience* **8**, 844-858 (2007).
2. D. Saal, Y. Dong, A. Bonci, R. C. Malenka, Drugs of abuse and stress trigger a common synaptic adaptation in dopamine neurons. *Neuron* **37**, 577-582 (2003).
3. M. A. Ungless, J. L. Whistler, R. C. Malenka, A. Bonci, Single cocaine exposure in vivo induces long-term potentiation in dopamine neurons. *Nature* **411**, 583-587 (2001).
4. B. Pradier *et al.*, Persistent but Labile Synaptic Plasticity at Excitatory Synapses. *The Journal of neuroscience : the official journal of the Society for Neuroscience* **38**, 5750-5758 (2018).
5. K. Koga *et al.*, Impaired presynaptic long-term potentiation in the anterior cingulate cortex of Fmr1 knock-out mice. *The Journal of neuroscience : the official journal of the Society for Neuroscience* **35**, 2033-2043 (2015).
6. C. A. Barnes *et al.*, LTP saturation and spatial learning disruption: effects of task variables and saturation levels. *The Journal of neuroscience : the official journal of the Society for Neuroscience* **14**, 5793-5806 (1994).
7. B. W. Schroeder, P. Shinnick-Gallagher, Fear learning induces persistent facilitation of amygdala synaptic transmission. *The European journal of neuroscience* **22**, 1775-1783 (2005).
8. R. Remedios *et al.*, Social behaviour shapes hypothalamic neural ensemble representations of conspecific sex. *Nature* **550**, 388-392 (2017).
9. Y. Li *et al.*, Neuronal Representation of Social Information in the Medial Amygdala of Awake Behaving Mice. *Cell* **171**, 1176-1190 e1117 (2017).
10. K. Keleman *et al.* (2012) Dopamine neurons modulate pheromone responses in Drosophila courtship learning. in *Nature* (Nature Publishing Group), pp 145-149.
11. X. Zhao, D. Lenek, U. Dag, B. J. Dickson, K. Keleman (2018) Persistent activity in a recurrent circuit underlies courtship memory in Drosophila. in *Elife* (eLife Sciences Publications Limited).
12. L. C. Griffith, A. Ejima, Courtship learning in Drosophila melanogaster: diverse plasticity of a reproductive behavior. *Learn Mem* **16**, 743-750 (2009).
13. M. P. Donley, J. B. Rosen, Novelty and fear conditioning induced gene expression in high and low states of anxiety. *Learning & memory* **24**, 449-461 (2017).
14. R. C. Twining, J. E. Vantrease, S. Love, M. Padival, J. A. Rosenkranz, An intra-amygdala circuit specifically regulates social fear learning. *Nature neuroscience* **20**, 459-469 (2017).
15. C. T. Gross, N. S. Canteras, The many paths to fear. *Nature reviews. Neuroscience* **13**, 651-658 (2012).
16. E. W. Fish, J. F. De Bold, K. A. Miczek, Aggressive behavior as a reinforcer in mice: activation by allopregnanolone. *Psychopharmacology* **163**, 459-466 (2002).
17. A. L. Falkner, L. Grosenick, T. J. Davidson, K. Deisseroth, D. Lin, Hypothalamic control of male aggression-seeking behavior. *Nature neuroscience* **19**, 596-604 (2016).
18. S. A. Golden *et al.*, Nucleus Accumbens Drd1-Expressing Neurons Control Aggression Self-Administration and Aggression Seeking in Mice. *The Journal of neuroscience : the official journal of the Society for Neuroscience* **39**, 2482-2496 (2019).
19. K. L. Gobrogge, Y. Liu, X. Jia, Z. Wang, Anterior hypothalamic neural activation and neurochemical associations with aggression in pair-bonded male prairie voles. *THE JOURNAL OF COMPARATIVE NEUROLOGY* **502**, 1109-1122 (2007).
20. M. Zelikowsky *et al.*, The Neuropeptide Tac2 Controls a Distributed Brain State Induced by Chronic Social Isolation Stress. *Cell* **173**, 1265-1279 e1219 (2018).
21. D. W. Kim *et al.*, Multimodal Analysis of Cell Types in a Hypothalamic Node Controlling Social Behavior. *Cell* **179**, 713-728 e717 (2019).

22. E. J. Hermans, N. F. Ramsey, J. van Honk, Exogenous testosterone enhances responsiveness to social threat in the neural circuitry of social aggression in humans. *Biological psychiatry* **63**, 263-270 (2008).
23. K. K. Soma, Testosterone and aggression: Berthold, birds and beyond. *Journal of neuroendocrinology* **18**, 543-551 (2006).
24. J. M. Hume, K. E. Wynne-Edwards, Castration reduces male testosterone, estradiol, and territorial aggression, but not paternal behavior in biparental dwarf hamsters (Phodopus campbelli). *Hormones and behavior* **48**, 303-310 (2005).
25. D. J. Albert, R. H. Jonik, N. V. Watson, B. B. Gorzalka, M. L. Walsh, Hormone-dependent aggression in male rats is proportional to serum testosterone concentration but sexual behavior is not. *Physiology & behavior* **48**, 409-416 (1990).
26. D. J. Albert, E. M. Dyson, M. L. Walsh, Intermale social aggression: reinstatement in castrated rats by implants of testosterone propionate in the medial hypothalamus. *Physiology & behavior* **39**, 555-560 (1987).
27. H. D. Steklis, G. L. Brammer, M. J. Raleigh, M. T. McGuire, Serum testosterone, male dominance, and aggression in captive groups of vervet monkeys (Cercopithecus aethiops sabaeus). *Hormones and behavior* **19**, 154-163 (1985).
28. X. Zha *et al.*, VMHvl-Projecting Vglut1+ Neurons in the Posterior Amygdala Gate Territorial Aggression. *Cell reports* **31** (2020).
29. T. Yamaguchi *et al.*, Posterior amygdala regulates sexual and aggressive behaviors in male mice. *Nature neuroscience* 10.1038/s41593-020-0675-x (2020).
30. L. Lo *et al.*, Connectional architecture of a mouse hypothalamic circuit node controlling social behavior. *Proceedings of the National Academy of Sciences of the United States of America* **116**, 7503-7512 (2019).
31. J. Nordman *et al.*, Potentiation of divergent medial amygdala pathways drives experience-dependent aggression escalation. *The Journal of neuroscience : the official journal of the Society for Neuroscience* 10.1523/JNEUROSCI.0370-20.2020 (2020).
32. S. Inoue *et al.*, Periodic Remodeling in a Neural Circuit Governs Timing of Female Sexual Behavior. *Cell* **179**, 1393-+ (2019).
33. H. Lee *et al.*, Scalable control of mounting and attack by Esr1+ neurons in the ventromedial hypothalamus. *Nature* **509**, 627-632 (2014).
34. L. Petreanu, T. Mao, S. M. Sternson, K. Svoboda, The subcellular organization of neocortical excitatory connections. *Nature* **457**, 1142-1145 (2009).
35. J. Lu *et al.*, MIN1PIPE: A Miniscope 1-Photon-Based Calcium Imaging Signal Extraction Pipeline. *Cell reports* **23**, 3673-3684 (2018).
36. J. I. Sanders, A. Kepecs, A low-cost programmable pulse generator for physiology and behavior. *Frontiers in neuroengineering* **7**, 43 (2014).